Different Impacts of Madden–Julian Oscillation on Winter Rainfall over Southern China

Xiong CHEN[1], Jian LING[2,3*], Chongyin LI[1,2], Lifeng LI[1], and Minghao YANG[1]

1 *College of Meteorology and Oceanography, National University of Defense Technology, Nanjing* 211101
2 *State Key Laboratory of Numerical Modeling for Atmospheric Sciences and Geophysical Fluid Dynamics, Institute of Atmospheric Physics, Chinese Academy of Sciences, Beijing* 100029
3 *University of Chinese Academy of Sciences, Chinese Academy of Sciences, Beijing* 100049

(Received July 24, 2020; in final form December 4, 2020)

ABSTRACT

Winter rainfall over southern China is usually enhanced when Madden–Julian oscillation (MJO) is active over the Indian Ocean, but it can be weakened under certain conditions. Here, the diversity of MJO impacts on winter rainfall and its mechanisms are explored by using scenarios of enhanced and suppressed rainfall anomalies over southern China when MJO is active over the Indian Ocean. The combined effects of low-frequency background moisture and intraseasonal winds are the major contributors to the different rainfall anomalies. Anomalous circulation in mid–high latitudes, especially on intraseasonal timescales, is almost opposite in the two scenarios, which can modulate the response of extratropical atmosphere to MJO heating and then induces the different circulations over southern China. In the enhanced scenario, mid–high latitudes of Eurasia and southern China are dominated by positive and negative sea level pressure anomalies, respectively. The southerly over southern China and the South China Sea induced by MJO heating promotes the anomalous moisture convergence and ascending motion over southern China, resulting in the enhanced rainfall. In the suppressed scenario, however, the circulation in mid–high latitudes does not favor rainfall over southern China and leads to the northerly response to MJO heating over southern China, which enhances moisture divergence and weakens rainfall over southern China.

Key words: Madden–Julian oscillation (MJO), winter rainfall, southern China, moisture diagnoses

Citation: Chen, X., J. Ling, C. Y. Li, et al., 2021: Different impacts of Madden–Julian oscillation on winter rainfall over southern China. *J. Meteor. Res.*, **35**(2), 271–281, doi: 10.1007/s13351-021-0138-7.

1. Introduction

Madden–Julian oscillation (MJO; Madden and Julian, 1971, 1972) is a planetary-scale variability in the tropical atmosphere that propagates eastward from the Indian Ocean to the central Pacific. The eastward speed and period of MJO are approximately 5 m s^{-1} and 30–90 days, respectively. As the dominant component of intraseasonal variability in the tropical atmosphere, the impacts of MJO on weather and climate systems can extend from the tropics to the extratropics (Zhang, 2013; Li C. Y. et al., 2014; Li T. et al., 2020). Rainfall in many regions around the world shows substantial variation on intraseasonal timescale corresponding to the location of MJO convection during its eastward propagation (Zhang et al., 2009; Liu and Yang, 2010; Jia et al., 2011). The onset and withdrawal of the South China Sea (SCS) summer monsoon are closely related to active and suppressed MJO convection over the equatorial Indian Ocean and SCS (Wang et al., 2018; Hu et al., 2020a, b). MJO activities over the western Pacific can also modulate the evolution of El Niño events (Hendon et al., 2007; Chen et al., 2016).

The winter rainfall belt in eastern China is over the Yangtze River basin during MJO convection over the Indian Ocean, and migrates towards South China when MJO convection enters the central Pacific (Liu and Yang, 2010). Active MJO convection over the Indian Ocean would favor a wet period over East Asia (Jeong et al., 2008; Kim et al., 2020) and southern China (Yuan and

Supported by the National Key Research and Development Program of China (2018YFA0606203 and 2018YFC1505901), National Natural Science Foundation of China (41520104008, 41922035, 41575062, and 41475070), and Key Research Program of Frontier Sciences of Chinese Academy of Sciences (QYZDB-SSW-DQC017).

*Corresponding author: lingjian@lasg.iap.ac.cn

© The Chinese Meteorological Society and Springer-Verlag Berlin Heidelberg 2021

Yang, 2010; Jia et al., 2011), while active MJO convection over the western Pacific would result in a dry period there. The amplitude of rainfall over southern China is twice as large as the winter mean when MJO is over the Indian Ocean (Jia et al., 2011). The impacts of MJO on rainfall are confined to the south of the Yangtze River in winter, while they can extend into larger southern regions and the Tibetan Plateau in summer (Ren and Shen, 2016). Summer rainfall over southeastern China increases by 15% when MJO is active over the Maritime Continent and decreases by 13% when MJO is active over the western Pacific (Zhang et al., 2009). Wang et al. (2017) found that the boreal summer intraseasonal oscillation (BSISO) also contributed to the interdecadal increases of rainfall over southern China around 1992/1993. In spring and pre-flood season (April–June), rainfall over South China and Yangtze River basin also shows systematic changes associated with the eastward propagation of MJO (Zhang et al., 2011; Bai et al., 2013). A recent study has indicated that MJO can modulate the intraseasonal variations of the diurnal cycle of coastal rainfall over South China (Chen et al., 2019).

MJO can modulate the occurrence probability of extreme rainfall in China (Hsu et al., 2016; Ren et al., 2018). The occurrence probability of 90th extreme summer rainfall increases over the Yangtze River basin with a magnitude of more than 40%, but decreases over South China when BSISO is over the eastern Indian Ocean (Ren et al., 2018). The occurrence probability of extreme winter rainfall events over southern China increases by 30%–50% relative to the winter mean when MJO is over the Indian Ocean, while it drops by 20%–40% when MJO enters the Pacific (Ren and Ren, 2017). MJO's influence on extreme rainfall is related to its amplitude: a stronger MJO tends to exert greater influences (Xavier et al., 2014).

MJO can also impact the persistent rainfall events in China. Persistent activity of MJO over the Indian Ocean was crucial to the continuous blizzard in January 2008 and November 2009 via regulating the continuous and vigorous moisture transport (Wu et al., 2009; Jia and Liang, 2013). In 1996, wet phase locking of the intraseasonal oscillation (ISO) and quasi-biweekly oscillation resulted in a prolonged wet episode from late June to mid-July (Li et al., 2015). The activity of three MJO episodes in summer 2016 was responsible for the intraseasonal variation of rainfall over the Yangtze River basin and North China (Shao et al., 2018).

The main ways in which MJO modulates rainfall in China are by regulating vertical motion and moisture transport (Zhang et al., 2009; Liu and Yang, 2010; Jia et al., 2011; Ren and Shen, 2016), summarized as the remote and local dynamical mechanisms by Zhang et al. (2009). Anomalous vertical motion over the Maritime Continent and western Pacific related to MJO can induce an anomalous local Hadley circulation over East Asia and lead to anomalous vertical motion and moisture transport in China (Zhang et al., 2009; He et al., 2011; Jia et al., 2011). MJO can also be considered as a diabatic heating source in the tropical atmosphere, which will induce a Gill-pattern anomalous circulation and influence the rainfall in China through the associated Rossby and Kelvin wave components (Zhang et al., 2009; Liu and Yang, 2010; He et al., 2011).

The influence of MJO over the Indian Ocean on winter rainfall in China is more prominent than its other phases (Jia et al., 2011; Chen et al., 2020a). Figure 1 shows the intraseasonal rainfall over southern China as a function of the amplitude of MJO over the Indian Ocean. It clearly shows that the positive rainfall anomaly has a greater chance of occurring when MJO convection is over the Indian Ocean, especially for the stronger MJO activity. However, quite a lot of days with strong negative rainfall anomaly are also noticed when enhanced MJO activity is over the Indian Ocean. This result may suggest that the impacts of MJO on the winter rainfall over southern China could be modulated by other climate systems. On interannual timescale, the impacts of MJO are modulated by some low-frequency climate systems (Chen et al., 2020b). Kim et al. (2020) found that rainfall anomalies induced by MJO over southern China and Japan are approximately 40% stronger in the easterly phase of quasi-biennial oscillation (QBO) than in its westerly phase. Significantly enhanced rainfall is observed over southern China when MJO convection is

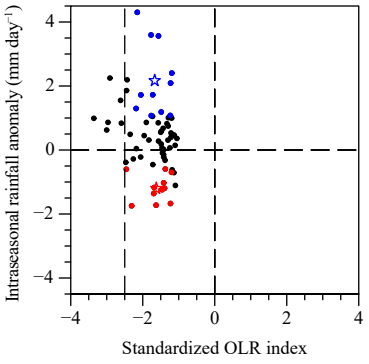

Fig. 1. Scatterplot of the intraseasonal rainfall anomaly (mm day^{-1}) and standardized Madden–Julian oscillation (MJO) outgoing longwave radiation (OLR) index for the 68 MJO cases. Blue and red indicate the selected enhanced and suppressed scenarios, respectively. Stars are the mean for both scenarios.

over the Indian Ocean in El Niño winter, but in La Niña winter, it only occurs in Zhejiang Province and adjacent areas (Chen et al., 2020a). However, if we consider the individual MJO events over the Indian Ocean rather than the seasonal mean, rainfall anomaly over southern China when MJO is over the Indian Ocean is not closely related to the phases of QBO or El Niño–Southern Oscillation (ENSO). Why could the impacts of moderate MJO on winter rainfall over southern China be different, and what regulates the impacts of individual MJO events? In this paper, we will explore the variations of the impacts of MJO on winter rainfall over southern China when MJO convection is over the Indian Ocean, and examine the reasons for these variations. The remainder of this paper is organized as follows. Section 2 briefly describes the data and methods. The variations of impacts of MJO on winter rainfall over southern China are presented in Section 3, and their causes are investigated in Section 4 through the analysis of anomalous large-scale atmospheric circulation, moisture transport, and influences of circulation in mid–high latitudes. Finally, the conclusions and discussion are provided in Section 5.

2. Data and methods

Daily rainfall data from more than 2000 stations in the Chinese mainland were collected and compiled by the National Meteorological Information Center of the China Meteorological Administration. Daily sea level pressure (SLP), three-dimensional winds, and specific humidity at different pressure levels with a horizontal resolution of 1.5° × 1.5° were taken from the ECMWF Reanalysis (ERA)-Interim global atmospheric reanalysis datasets produced by the ECMWF (Dee et al., 2011). Daily outgoing longwave radiation (OLR) data with a 2.5° × 2.5° horizontal resolution came from NOAA (Liebmann and Smith, 1996). All the datasets cover the period from 1 January 1979 to 31 December 2017. For all datasets, their climatology and long-time linear trend were firstly removed, and the MJO and ISO signals were obtained by using a 30–90-day Lanczos bandpass filter (Duchon, 1979; Chen et al., 2016). Only the MJO events in boreal winter (November–March) when its amplitude is larger than one standard deviation (Kim et al., 2014; Feng et al., 2015) are diagnosed in this study.

The index of MJO activity over the Indian Ocean is defined in terms of the intraseasonal OLR averaged over 10°S–10°N, 65°–95°E. An active MJO event over the Indian Ocean is identified if the index is lower than one standard deviation for at least five consecutive days; day 0 is the day with maximum amplitude. In this way, 68 MJO cases were identified. The intraseasonal rainfall anomalies over southern China (21°–31°N, 110°–122°E) on day 0 for each MJO case are shown in Fig. 1. The results suggest that anomalous rainfall over southern China is positive for those strong MJO cases with maximum index exceeding 2.5 standard deviations, while the occurrence probability of negative rainfall anomalies over southern China is more than a third for the MJO cases whose maximum index is lower than that. To investigate the reasons for the different impacts of MJO with moderate amplitude over the Indian Ocean on winter rainfall over southern China, these MJO cases are classified into two scenarios. In one scenario, winter rainfall over southern China is enhanced when MJO is active over the Indian Ocean (refer to as the enhanced scenario), while in the other scenario, the rainfall is suppressed (refer to as the suppressed scenario; selected scenarios are listed in Table 1 and marked by blue and red in Fig. 1).

3. Characteristics of rainfall anomalies over southern China

Figure 2a shows the composite index of MJO activity for both scenarios. This indicates that significant MJO activity over the Indian Ocean is persistent from days −10 to 10 for both scenarios and there is no significant difference between them. Composite daily rainfall anomaly and its intraseasonal component averaged over southern China for the two scenarios are shown in Figs. 2b, c, respectively. Daily rainfall exhibits strong variability during both scenarios and is also characterized by noticeable features of intraseasonal oscillation. Anomalous intraseasonal rainfall can persist for about 20 days from days −10 to 10, which coincides with the variations of MJO activity over the Indian Ocean (Fig. 2a). The intensity of positive rainfall anomalies in the enhanced scenario is significantly stronger than that for the negative rainfall anomalies in the suppressed scenario.

Figure 3 displays the composite anomalous in-

Table 1. Day 0 for both rainfall anomaly scenarios

No.	Enhanced (yyyy-mm-dd)	Suppressed
1	1986-03-17	1980-01-09
2	1990-02-26	1984-11-24
3	1991-12-25	1985-11-06
4	1996-03-25	1994-11-19
5	2006-01-12	2001-11-13
6	2008-02-01	2002-11-12
7	2009-11-07	2010-11-25
8	2012-03-04	2010-12-31
9	2012-12-28	2014-12-23
10	2013-02-12	2015-02-06
11	2016-11-23	2017-03-01

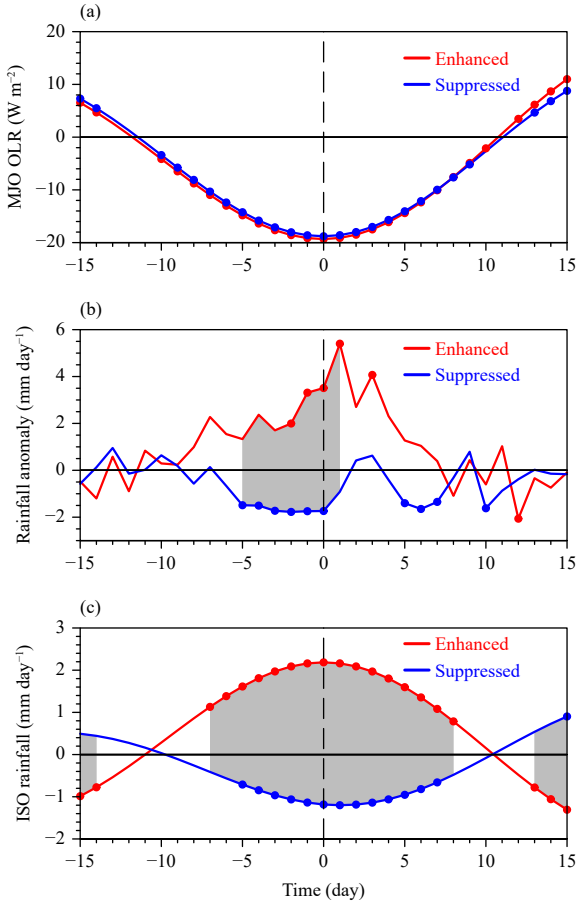

Fig. 2. Composite daily anomalies of (a) MJO OLR (W m^{-2}) averaged over the Indian Ocean (10°S–10°N, 65°–95°E), (b) total rainfall, and (c) intraseasonal rainfall averaged over southern China (mm day^{-1}) for the enhanced (red line) and suppressed (blue line) scenarios. Dots and gray shading indicate that the results for composites and their difference are significant at the 90% confidence level, respectively.

traseasonal rainfall on day 0 for the two scenarios. Significant rainfall anomalies for both are located mainly over southern China (Jiangxi, Fujian, and Zhejiang provinces). The maximum amplitude of rainfall anomalies exceeds 2 mm day^{-1} for both scenarios, which is almost the same as the rainfall climatology when MJO convection is over the Indian Ocean (Jia et al., 2011; Chen et al., 2020a). The intensity of positive rainfall anomalies in the enhanced scenario is slightly greater than that for the negative rainfall anomalies in the suppressed scenario. The difference in intraseasonal rainfall between these two scenarios also reveals that active MJO over the Indian Ocean could result in significantly different rainfall over southern China (Fig. 3c).

The above results indicate that rainfall anomalies over southern China differ significantly between the two scenarios. However, there are not significant differences in the intensity of MJO activity over the Indian Ocean (Figs. 1, 2a). What causes the different rainfall anomalies over southern China when MJO is active over the Indian Ocean? In the following sections, we will explore this question from the perspective of large-scale atmospheric circulation, moisture transport, and influences of circulation in mid–high latitudes.

4. Causes of different rainfall anomalies

4.1 *Features of large-scale atmospheric circulation*

Figure 4 shows composite anomalous circulation at 850 hPa and SLP on day 0 for both scenarios. Anomalous circulation for both scenarios is quite similar in the tropics. Anomalous easterlies prevail from the central Pacific to the eastern Indian Ocean and anomalous westerlies are located over the western equatorial Indian Ocean. However, anomalous circulation in the extratropics differs significantly between scenarios. There is strong anomalous southwesterlies over the SCS in the enhanced scenario, which results in the convergence over southern

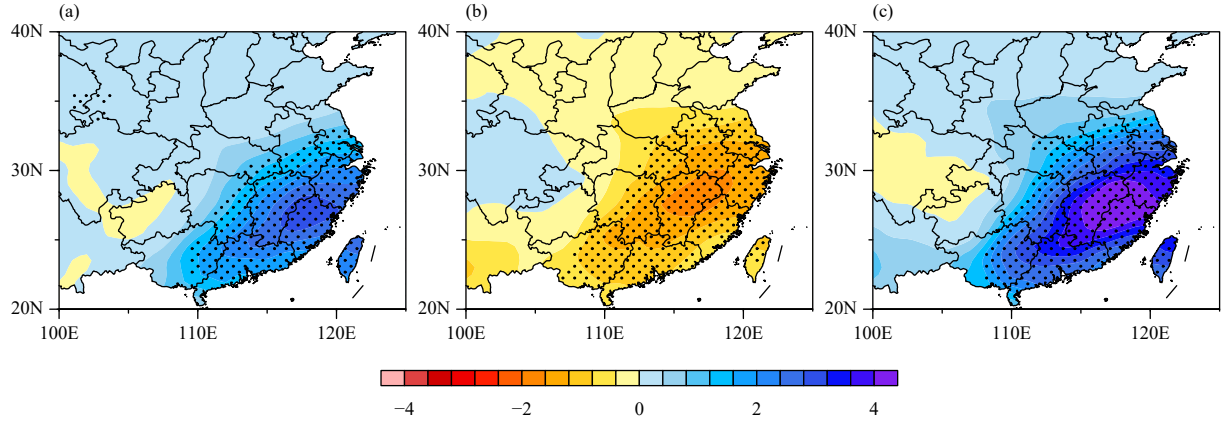

Fig. 3. Composite anomalous intraseasonal rainfall (mm day^{-1}) for the (a) enhanced and (b) suppressed scenarios, and (c) their differences over China on day 0. The results significant at the 90% confidence level are stippled.

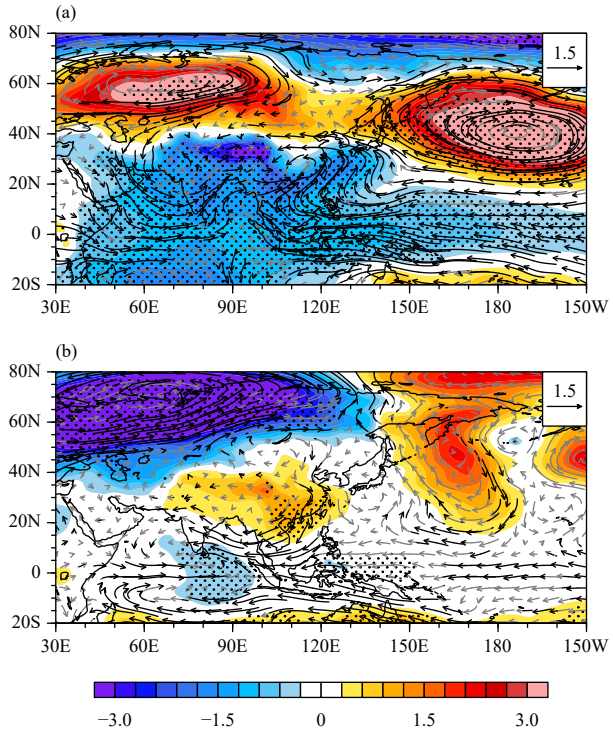

Fig. 4. Composite anomalous intraseasonal sea level pressure (SLP) (color; hPa) and winds at 850 hPa (vector; m s^{-1}) on day 0 for the (a) enhanced and (b) suppressed scenarios. Results significant at the 90% confidence level are stippled for SLP and marked in black for vectors.

China and favors rainfall (Fig. 4a). However, in the suppressed scenario, southern China is dominated by an anomalous northerly and positive SLP (Fig. 4b). Meanwhile, anomalous positive SLP and anticyclonic circulation dominate most parts of mid–high latitude Eurasian regions in the enhanced scenario (Fig. 4a), and these same regions are controlled by anomalous negative SLP and cyclonic circulation in the suppressed scenario (Fig. 4b).

Composite anomalous meridional–vertical circulation averaged over 110°–120°E shows that vertical circulation also differs noticeably between the two scenarios (Fig. 5). In the enhanced scenario, a distinct local anomalous Hadley circulation over East Asia is identified with a strong anomalous ascending motion over eastern China and an anomalous descending motion in the tropics near 10°N. The vertical motion can extend from the lower troposphere to the upper troposphere. The southerly from the tropics and the northerly from the middle latitudes below 850 hPa merge over southern China, which contributes to the convergence and ascending motion there (Fig. 5a). In the suppressed scenario, the descending motion in the tropics is not noticeable and the equatorial region is dominated by an ascending motion. Over southern China, an anomalous descending motion and northerly prevail in the whole troposphere. Unlike the enhanced scenario, there is no local anomalous Hadley circulation over East Asia in the suppressed scenario.

The quasi-geostrophic vertical motion is controlled by the vertical derivation of horizontal advection of geostrophic vorticity, the horizontal Laplacian of thermal advection, and diabatic heating (Jeong et al., 2008). The warm (cold) thermal advection and diabatic heating

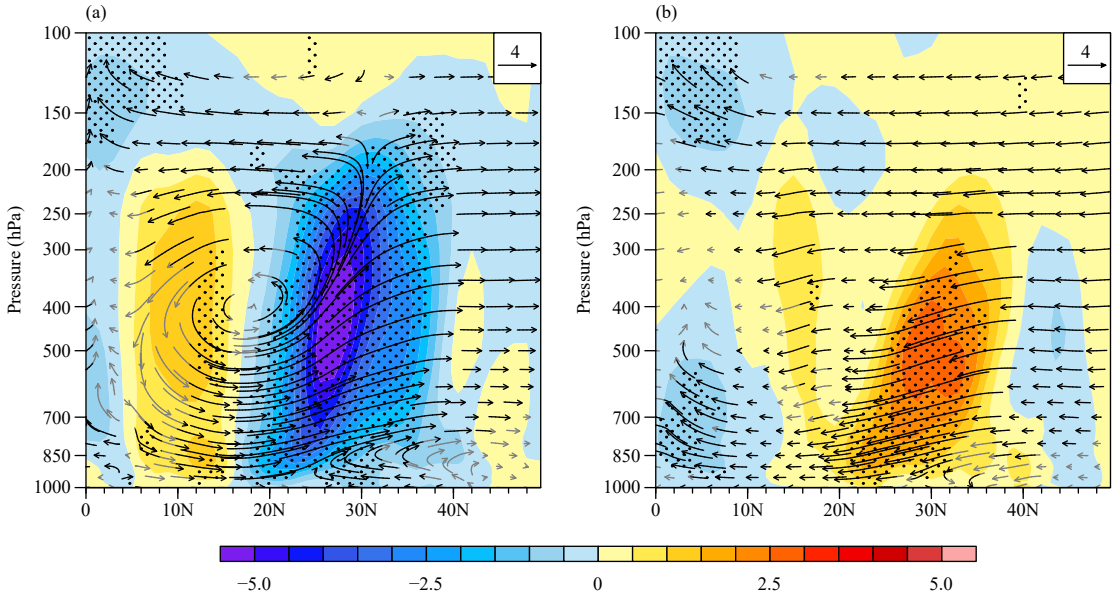

Fig. 5. Composite anomalous intraseasonal meridional–vertical circulation (vector; horizontal: m s^{-1}, vertical: Pa s^{-1}; vertical velocity multiplied by 500) and vertical velocity (color; 10^{-2} Pa s^{-1}) averaged over 110°–120°E on day 0 for the (a) enhanced and (b) suppressed scenarios. Results significant at the 90% confidence level are stippled for vertical velocity and marked in black for vectors.

(cooling) will induce the anomalous ascending (descending) motion. The anomalous vertical motion, thermal advection, and diabatic heating at 500 hPa averaged over southern China for the two scenarios are shown in Table 2. The warm (cold) thermal advection of low-frequency background air temperature by the anomalous southerly (northerly) and the diabatic heating (cooling) over southern China induced by MJO forcing will lead to the ascending (descending) motion there in the enhanced (suppressed) scenario.

4.2 *Moisture transport*

Composite anomalous moisture flux and its divergence integrated from 1000 to 500 hPa for the two different scenarios are shown in Fig. 6. Southwest flow can transport moisture from the tropical Indian Ocean, SCS, and western Pacific into the Chinese mainland, and lead to moisture convergence over southern China in the enhanced scenario (Fig. 6a). However, in the suppressed scenario, an anomalous northeasterly over southern China leads to significant moisture divergence there (Fig. 6b).

Table 2. Anomalous intraseasonal vertical motion, thermal advection, and diabatic heating at 500 hPa averaged over southern China for the two scenarios

Scenario	Omega (10^{-2} Pa s^{-1})	Thermal advection (10^{-5} K s^{-1})	Diabatic heating (10^{-6} K s^{-1})
Enhanced	−4.0	−1.36	9.71
Suppressed	1.5	0.84	−2.83

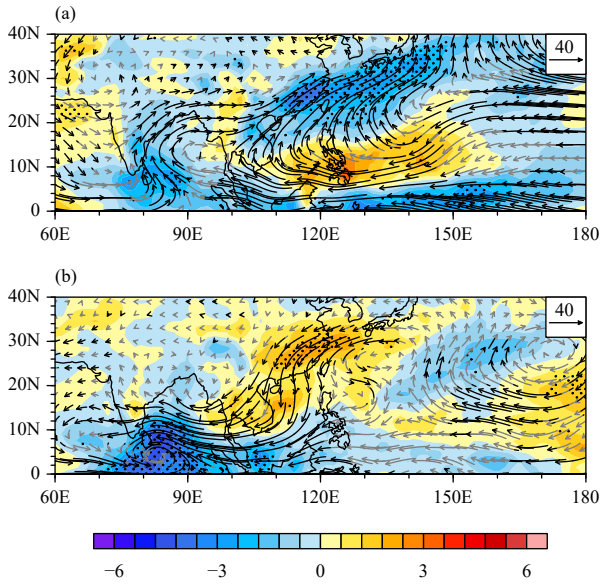

Fig. 6. Composite vertical integrated (from 1000 to 500 hPa) anomalous intraseasonal moisture flux (vector; 10^{-3} kg m^{-1} s^{-1}) and its divergence (color; 10^{-8} kg m^{-2} s^{-1}) on day 0 for the (a) enhanced and (b) suppressed scenarios. Results significant at the 90% confidence level are stippled for divergence and marked in black for moisture flux.

Moisture flux divergence is composed of zonal moisture convergence and advection, and meridional moisture convergence and advection, which can be written as (Chen et al., 2020a, b):

$$M_{\rm div} = q\frac{\partial u}{\partial x} + u\frac{\partial q}{\partial x} + q\frac{\partial v}{\partial y} + v\frac{\partial q}{\partial y}, \quad (1)$$

where q, u, and v represent the specific humidity, zonal velocity, and meridional velocity, respectively; $M_{\rm div}$ is the moisture flux divergence. The four terms on the right-hand side of Eq. (1) are (from left to right) zonal moisture convergence, zonal moisture advection, meridional moisture convergence, and meridional moisture advection, respectively. Diagnoses of moisture flux divergence indicate that anomalous moisture flux divergence is mainly attributed to the meridional moisture convergence in the enhanced scenario (Fig. 7). However, zonal moisture convergence, and meridional moisture convergence and advection make similar contribution to the moisture flux divergence in the suppressed scenario. Zonal moisture advection hinders the moisture flux convergence (divergence) in the enhanced (suppressed) scenario.

The specific humidity and zonal and meridional velocity can be further decomposed into three components according to their timescales, the high-frequency (with a period < 30 days) component, intraseasonal (MJO/ISO; 30–90 days) component, and low-frequency background state (LFBS; with a period > 90 days) component following Chen et al. (2016, 2020a, b):

$$q = q^* + q' + \bar{q},\ u = u^* + u' + \bar{u},\ v = v^* + v' + \bar{v}, \quad (2)$$

where the asterisk, prime, and overbar denote the high-frequency, MJO/ISO, and LFBS components, respectively. Thus, the four terms on the right-hand side of Eq. (1) can be further written as:

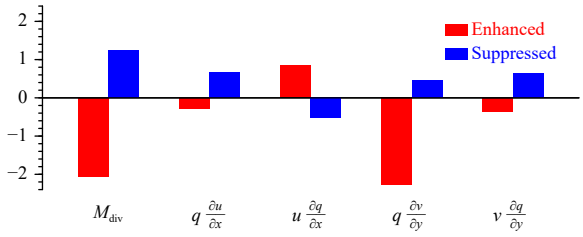

Fig. 7. Composite vertical integral (from 1000 to 500 hPa; 10^{-8} kg m^{-2} s^{-1}) of individual terms in Eq. (1) averaged over 21°–31°N, 110°–120°E on day 0 for the enhanced (red) and suppressed (blue) scenarios.

$$q\frac{\partial u}{\partial x} = q^*\frac{\partial u^*}{\partial x} + q^*\frac{\partial u'}{\partial x} + q^*\frac{\partial \bar{u}}{\partial x} + q'\frac{\partial u^*}{\partial x} + q'\frac{\partial u'}{\partial x} + q'\frac{\partial \bar{u}}{\partial x} + \bar{q}\frac{\partial u^*}{\partial x} + \bar{q}\frac{\partial u'}{\partial x} + \bar{q}\frac{\partial \bar{u}}{\partial x}, \quad (3)$$

$$u\frac{\partial q}{\partial x} = u^*\frac{\partial q^*}{\partial x} + u^*\frac{\partial q'}{\partial x} + u^*\frac{\partial \bar{q}}{\partial x} + u'\frac{\partial q^*}{\partial x} + u'\frac{\partial q'}{\partial x} + u'\frac{\partial \bar{q}}{\partial x} + \bar{u}\frac{\partial q^*}{\partial x} + \bar{u}\frac{\partial q'}{\partial x} + \bar{u}\frac{\partial \bar{q}}{\partial x}, \quad (4)$$

$$q\frac{\partial v}{\partial y} = q^*\frac{\partial v^*}{\partial y} + q^*\frac{\partial v'}{\partial y} + q^*\frac{\partial \bar{v}}{\partial y} + q'\frac{\partial v^*}{\partial y} + q'\frac{\partial v'}{\partial y} + q'\frac{\partial \bar{v}}{\partial y} + \bar{q}\frac{\partial v^*}{\partial y} + \bar{q}\frac{\partial v'}{\partial y} + \bar{q}\frac{\partial \bar{v}}{\partial y}, \quad (5)$$

$$v\frac{\partial q}{\partial y} = v^*\frac{\partial q^*}{\partial y} + v^*\frac{\partial q'}{\partial y} + v^*\frac{\partial \bar{q}}{\partial y} + v'\frac{\partial q^*}{\partial y} + v'\frac{\partial q'}{\partial y} + v'\frac{\partial \bar{q}}{\partial y} + \bar{v}\frac{\partial q^*}{\partial y} + \bar{v}\frac{\partial q'}{\partial y} + \bar{v}\frac{\partial \bar{q}}{\partial y}. \quad (6)$$

The terms on the right-hand side of Eqs. (3)–(6) averaged over southern China are shown in Fig. 8. Results show that the zonal moisture divergence in the suppressed scenario is mainly induced by the LFBS moisture divergence caused by intraseasonal zonal wind (Fig. 8a). Zonal moisture advection is mainly dominated by the intraseasonal moisture advection caused by LFBS zonal wind, which leads to the moisture divergence (convergence) in the enhanced (suppressed) scenario (Fig. 8b). Meridional moisture convergence is the major contributor to the moisture convergence in the enhanced scenario, which mainly stems from the LFBS moisture convergence caused by intraseasonal meridional wind (Fig. 8c). Meridional moisture divergence is very weak in the suppressed scenario (Fig. 7), which is dominated by the high-frequency meridional wind and moisture (Fig. 8c). Meridional moisture advection also contributes to the moisture convergence (divergence) in the enhanced (suppressed) scenario (Fig. 7), which is mainly induced by the LFBS moisture advection caused by intraseasonal meridional wind (Fig. 8d). Therefore, the combination of moisture and circulation on different timescales, especially on the LFBS and intraseasonal timescales, leads to the differing moisture flux divergence over southern China.

4.3 *Influences of mid–high latitude circulation*

Anomalous intraseasonal circulation plays an important role in the anomalous moisture flux divergence in both scenarios. What induces their differing features of intraseasonal wind? MJO can be considered as a diabatic heating source in the tropical atmosphere, which will influence the rainfall over China via forcing anomalous circulation and vertical motion (Liu and Yang, 2010; He et al., 2011). Figure 9 shows the composite intraseasonal streamfunction and rotational winds at 850 hPa on day 0 for both scenarios. The responses of atmospheric circulation to MJO heating in the enhanced scenario are consistent with the theoretical result of Gill (1980). Westerly is located to the west of MJO heating and two cyclonic circulation gyres straddle it, which can be considered as the Rossby wave gyres. Equatorial Kelvin wave can also be found to the east of MJO heating. The easterly is located to the east of MJO heating and two anticyclonic circulation gyres straddle it. Southern China lies between the cyclonic and anticyclonic circulations, and the southwesterly can convey robust moisture towards China and lead to moisture convergence there, which favors rainfall over southern China (Liu and Yang, 2010; He et al., 2011). However, the Rossby wave response is not prom-

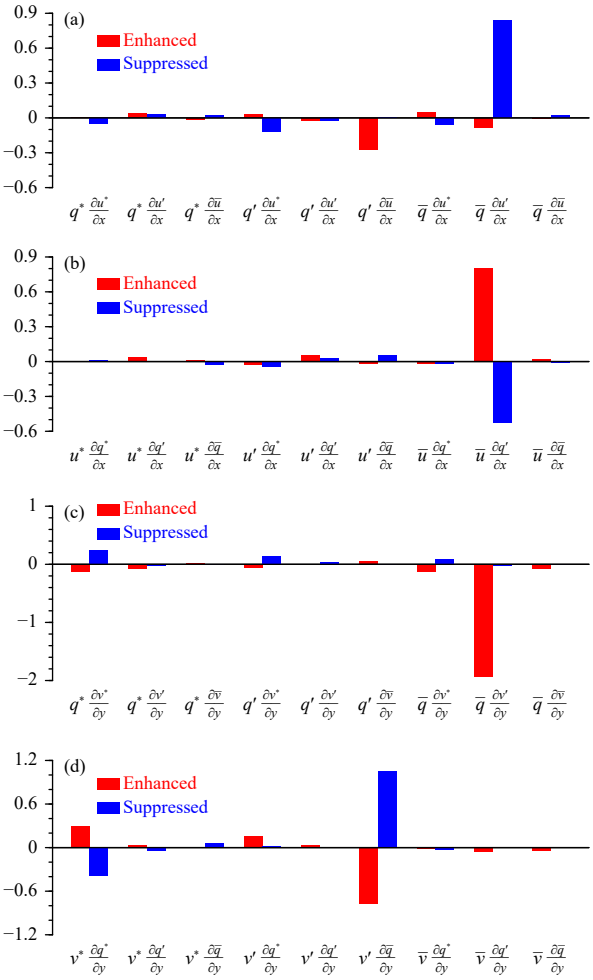

Fig. 8. Composite vertical integral (from 1000 to 500 hPa; 10^{-8} kg m^{-2} s^{-1}) of individual terms in the scale decomposition equations for (a) zonal moisture convergence, (b) zonal moisture advection, (c) meridional moisture convergence, and (d) meridional moisture advection averaged over 21°–31°N, 110°–120°E on day 0 for the enhanced (red) and suppressed (blue) scenarios.

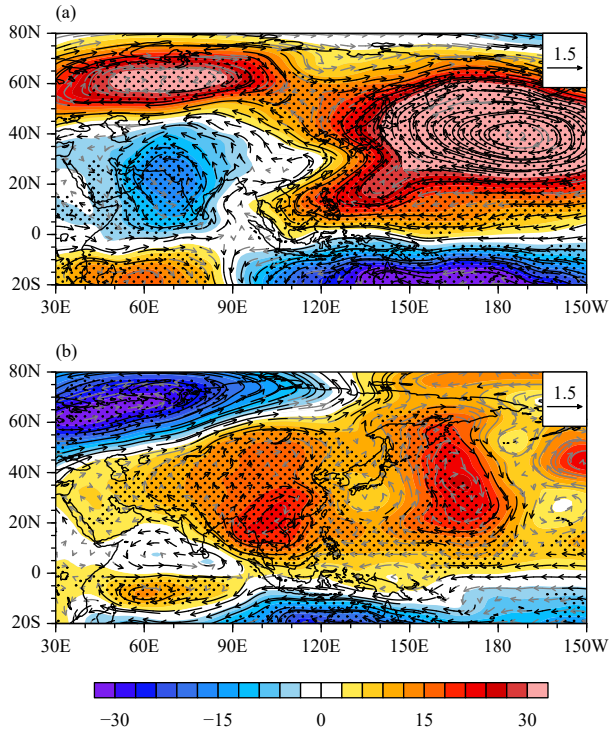

Fig. 9. Composite anomalous intraseasonal streamfunction (color; 10^5 m^2 s^{-1}) and rotational winds at 850 hPa (vector; m s^{-1}) on day 0 for the (a) enhanced and (b) suppressed scenarios. Results significant at the 90% confidence level are stippled for streamfunction and marked in black for rotational winds.

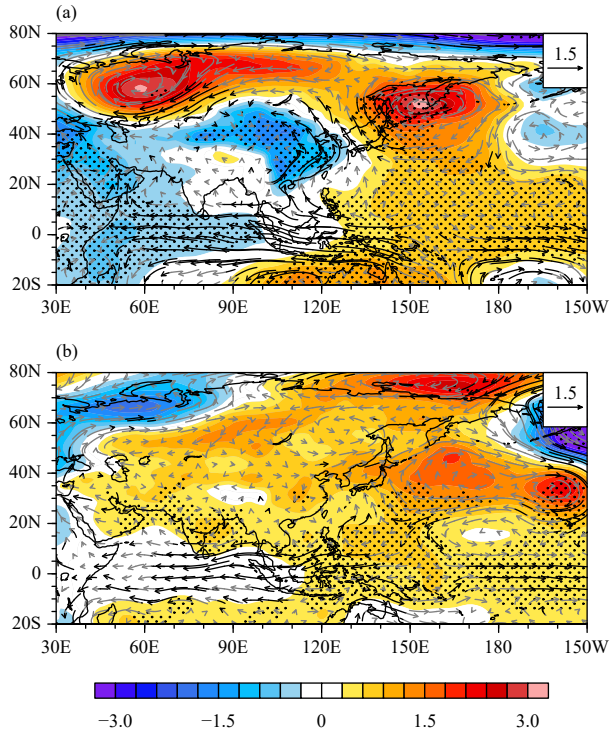

Fig. 10. As in Fig. 4, but for day −10.

inent in the suppressed scenario (Fig. 9b). The cyclonic circulation to the north of the equator is very weak and cannot influence rainfall over China. Southern China is controlled by the anticyclonic circulation and positive streamfunction anomalies, which results in the anomalous northerly flow and moisture divergence over the region.

Different responses of atmospheric circulation over southern China to MJO heating may be attributed to the different circulation over mid–high latitude Eurasia, because the influences of MJO on the extratropics are regulated by the extratropical background flow (Bao and Hartmann, 2014; Lin and Brunet, 2018; Zheng and Chang, 2020). Composites of intraseasonal circulation and SLP on day −10 are shown in Fig. 10. Some anomalous circulation features similar to those on day 0 can be observed on day −10 when MJO convection is just occurring over the Indian Ocean, such as the negative SLP anomalies over southern China and positive SLP anomalies over the Ural region in the enhanced scenario, and the positive SLP anomalies over southern China and negative SLP anomalies over the Novaya Zemlya region in the suppressed scenario. Figure 11a displays the evolution of intraseasonal SLP averaged over southern China, which is leading the variation of rainfall anomalies over southern China and MJO activity over the Indian Ocean about five days. Intraseasonal SLP over southern China is not significant after day 2. Rainfall and moisture convergence anomalies over southern China are almost in-phase with MJO activity over the Indian Ocean (Figs. 2,

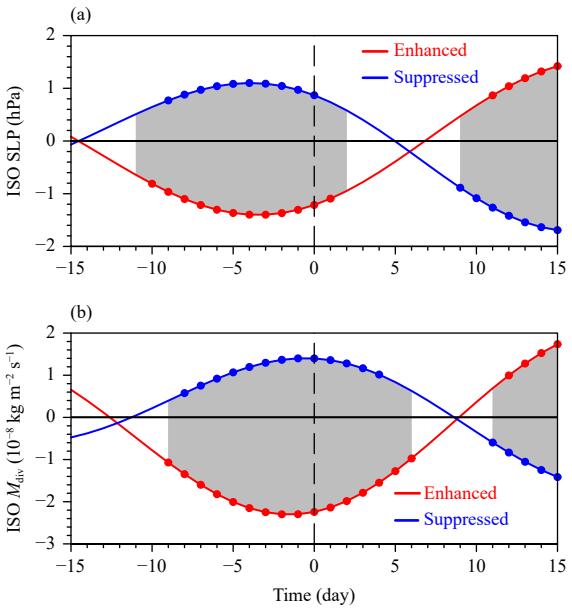

Fig. 11. As in Fig. 2c, but for the intraseasonal (a) SLP (hPa) and (b) moisture flux divergence (10^{-8} kg m^{-2} s^{-1}) averaged over southern China.

11b). Therefore, we speculate that the variation of rainfall over southern China is mainly controlled by the circulation related to MJO. Different background states over the mid–high latitudes could lead to the different distributions of MJO-related circulation even though the intensity of MJO convection is the same. Different circulation induced by MJO will therefore lead to the different rainfall over southern China when MJO is active over the Indian Ocean.

5. Conclusions and discussion

MJO has significant influences on winter rainfall over southern China and is a major source of predictability for the intraseasonal rainfall over the region. In general, rainfall over southern China is enhanced when MJO is active over the Indian Ocean. However, the impacts of MJO with moderate amplitude on winter rainfall over southern China could be different due to other factors. Based on diagnoses of rainfall, circulation, moisture transport, and the effects of mid–high latitude circulation, this paper explored the different impacts of MJO over the Indian Ocean on winter rainfall over southern China.

While the strongest MJO convection over the Indian Ocean can induce positive rainfall anomalies over southern China, more than one-third moderate MJO convection over the Indian Ocean is corresponding to the negative rainfall anomalies over southern China. Two different scenarios of rainfall anomalies over southern China when moderate MJO is active over the Indian Ocean were identified. Rainfall over southern China is significantly enhanced (weakened) in enhanced (suppressed) scenario. The center of anomalous rainfall is mainly located in Jiangxi, Fujian, and Zhejiang provinces for both scenarios. The maximum amplitude of rainfall anomalies exceeds 2 mm day^{-1} for both scenarios, which is almost the same as the rainfall climatology when MJO is active over the Indian Ocean. Rainfall anomalies are closely linked to the anomalous circulation and moisture transport. In the enhanced scenario, mid–high latitude Eurasia is dominated by anomalous anticyclonic circulation and positive SLP, and the southern China is controlled by negative SLP anomalies. In the suppressed scenario, positive SLP anomalies are located over southern China and mid–high latitude Eurasia is dominated by anomalous cyclonic circulation and negative SLP. Anomalous circulation can modulate the circulation and convergence over southern China. More importantly, they lead to the different responses of atmospheric circulation to the MJO heating. Anomalous southwesterly over the SCS forced by MJO heating can transport robust moisture from the tropics into the Chinese mainland and promote the anomalous ascending motion there in the enhanced scenario. In the suppressed scenario, however, MJO forces an anomalous northeasterly over southern China and the SCS, which induces the moisture divergence over southern China and weakens rainfall there. The combined effects of moisture and circulation on different timescales, especially on the LFBS and intraseasonal timescales, lead to the different moisture flux divergence between these two scenarios. Moisture convergence in the enhanced scenario is dominated by meridional moisture convergence, especially the LFBS moisture convergence caused by intraseasonal meridional wind. Zonal moisture divergence, and meridional moisture divergence and advection make a similar contribution to the moisture divergence in the suppressed scenario, and they are mainly attributed to the LFBS moisture divergence caused by intraseasonal zonal wind, high-frequency moisture divergence caused by high-frequency meridional wind, and the LFBS moisture advection caused by intraseasonal meridional wind, respectively.

Do the different impacts of MJO on rainfall over southern China stem from the differences in MJO itself? If we consider MJO as a heating forcing of atmosphere, it will induce similar circulation anomalies under the same background flow for the MJO events with the same amplitude. Only the MJO itself cannot show distinct diversity of impacts on winter rainfall over southern China. For strong MJO events, its induced circulation anomalies are too strong to be modulated by the background flow, and they will enhance the rainfall over southern China. However, for moderate MJO events with comparable amplitude, their induced circulation could be modulated by the background flow and lead to the different rainfall anomalies over southern China. As can be seen in Fig. 9, the Rossby and Kelvin gyres of the MJO differ noticeably between the two scenarios, which may be due to the different circulation patterns over the mid–high latitudes. The anomalous circulation over East Asia, which directly modulates the rainfall over southern China, is due to the combined effects of the circulation over mid–high latitudes and the modulated MJO circulation. In addition, the anomalous circulation over East Asia may contribute to the differences in the suppressed convection over the western Pacific between the two scenarios and also regulate MJO propagation (Chen et al., 2017). More numerical experiments to confirm this conclusion will be carried out in further studies.

The LFBS can modulate the impacts of MJO on weather and climate systems (Chen et al., 2020a; Kim et

al., 2020). The background circulation is similar between the two scenarios (not shown), but the intraseasonal circulation differs significantly (Figs. 4, 10). Therefore, the intraseasonal circulation can also regulate the response of atmosphere to MJO heating, and this should be considered when forecasting MJO activity and its influences. What controls the intraseasonal circulation variability over mid–high latitude regions of Eurasia merits further study.

Acknowledgments. The daily rainfall data from stations in southern China were provided by the National Meteorological Information Center of the China Meteorological Administration (http://data.cma.cn/). Daily atmospheric data were obtained from the ERA-Interim global atmospheric reanalysis datasets (https://www.ecmwf.int/). Interpolated daily OLR data were provided by NOAA (https://psl.noaa.gov/).

REFERENCES

Bai, X.-X., C.-Y. Li, Y.-K. Tan, et al., 2013: The impacts of Madden–Julian Oscillation on spring rainfall in East China. *J. Trop. Meteor.*, **19**, 214–222, doi: 10.16555/j.1006-8775.2013.03.002.

Bao, M., and D. L. Hartmann, 2014: The response to MJO-like forcing in a nonlinear shallow-water model. *Geophys. Res. Lett.*, **41**, 1322–1328, doi: 10.1002/2013GL057683.

Chen, X., J. Ling, and C. Y. Li, 2016: Evolution of the Madden–Julian oscillation in two types of El Niño. *J. Climate*, **29**, 1919–1934, doi: 10.1175/JCLI-D-15-0486.1.

Chen, X., C. Y. Li, J. Ling, et al., 2017: Impact of East Asian winter monsoon on MJO over the equatorial western Pacific. *Theor. Appl. Climatol.*, **127**, 551–561, doi: 10.1007/s00704-015-1649-x.

Chen, X., C. Y. Li, X. Li, et al., 2020a: Modulation of the impacts of Madden–Julian Oscillation on winter rainfall in China by El Niño-Southern Oscillation. *Int. J. Climatol.*, **40**, 4039–4052, doi: 10.1002/joc.6437.

Chen, X., C. Y. Li, L. F. Li, et al., 2020b: Interannual variations of the influences of MJO on winter rainfall in southern China. *Environ. Res. Lett.*, **15**, 114011, doi: 10.1088/1748-9326/abb7b0.

Chen, X. C., F. Q. Zhang, and J. H. Ruppert, 2019: Modulations of the diurnal cycle of coastal rainfall over South China caused by the boreal summer intraseasonal oscillation. *J. Climate*, **32**, 2089–2108, doi: 10.1175/JCLI-D-18-0786.1.

Dee, D. P., S. M. Uppala, A. J. Simmons, et al., 2011: The ERA-Interim reanalysis: configuration and performance of the data assimilation system. *Quart. J. Roy. Meteor. Soc.*, **137**, 553–597, doi: 10.1002/qj.828.

Duchon, C. E., 1979: Lanczos filtering in one and two dimensions. *J. Appl. Meteor.*, **18**, 1016–1022, doi: 10.1175/1520-0450(1979)018<1016:LFIOAT>2.0.CO;2.

Feng, J., T. Li, and W. J. Zhu, 2015: Propagating and nonpropagating MJO events over Maritime Continent. *J. Climate*, **28**, 8430–8449, doi: 10.1175/JCLI-D-15-0085.1.

Gill, A. E., 1980: Some simple solutions for heat-induced tropical circulation. *Quart. J. Roy. Meteor. Soc.*, **106**, 447–462, doi: 10.1002/qj.49710644905.

He, J. H., H. Lin, and Z. W. Wu, 2011: Another look at influences of the Madden-Julian Oscillation on the wintertime East Asian weather. *J. Geophys. Res. Atmos.*, **116**, D03109, doi: 10.1029/2010JD014787.

Hendon, H. H., M. C. Wheeler, and C. D. Zhang, 2007: Seasonal dependence of the MJO–ENSO relationship. *J. Climate*, **20**, 531–543, doi: 10.1175/JCLI4003.1.

Hsu, P.-C., J.-Y. Lee, and K.-J. Ha, 2016: Influence of boreal summer intraseasonal oscillation on rainfall extremes in southern China. *Int. J. Climatol.*, **36**, 1403–1412, doi: 10.1002/joc.4433.

Hu, P., W. Chen, S. F. Chen, et al., 2020a: Statistical analysis of the impacts of intra-seasonal oscillations on the South China Sea summer monsoon withdrawal. *Int. J. Climatol.*, **40**, 1919–1927, doi: 10.1002/joc.6284.

Hu, P., W. Chen, S. F. Chen, et al., 2020b: Extremely early summer monsoon onset in the South China Sea in 2019 following an El Niño event. *Mon. Wea. Rev.*, **148**, 1877–1890, doi: 10.1175/MWR-D-19-0317.1.

Jeong, J.-H., B.-M. Kim, C.-H. Ho, et al., 2008: Systematic variation in wintertime precipitation in East Asia by MJO-induced extratropical vertical motion. *J. Climate*, **21**, 788–801, doi: 10.1175/2007JCLI1801.1.

Jia, X.-L., and X.-Y. Liang, 2013: Possible impacts of Madden–Julian Oscillation on the severe rain-snow weather in China during November 2009. *J. Trop. Meteor.*, **19**, 233–241, doi: 10.16555/j.1006-8775.2013.03.004.

Jia, X. L., L. J. Chen, F. M. Ren, et al., 2011: Impacts of the MJO on winter rainfall and circulation in China. *Adv. Atmos. Sci.*, **28**, 521–533, doi: 10.1007/s00376-010-9118-z.

Kim, D., J.-S. Kug, and A. H. Sobel, 2014: Propagating versus nonpropagating Madden–Julian oscillation events. *J. Climate*, **27**, 111–125, doi: 10.1175/JCLI-D-13-00084.1.

Kim, H., S.-W. Son, and C. Yoo, 2020: QBO modulation of the MJO-related precipitation in East Asia. *J. Geophys. Res. Atmos.*, **125**, e2019JD031929, doi: 10.1029/2019JD031929.

Li, C. Y., J. Ling, J. Song, et al., 2014: Research progress in China on the tropical atmospheric intraseasonal oscillation. *J. Meteor. Res.*, **28**, 671–692, doi: 10.1007/s13351-014-4015-5.

Li, J. Y., J. Y. Mao, and G. X. Wu, 2015: A case study of the impact of boreal summer intraseasonal oscillations on Yangtze rainfall. *Climate Dyn.*, **44**, 2683–2702, doi: 10.1007/s00382-014-2425-9.

Li, T., J. Ling, and P.-C. Hsu, 2020: Madden–Julian Oscillation: Its discovery, dynamics, and impact on East Asia. *J. Meteor. Res.*, **34**, 20–42, doi: 10.1007/s13351-020-9153-3.

Liebmann, B., and C. A. Smith, 1996: Description of a complete (interpolated) outgoing longwave radiation dataset. *Bull. Amer. Meteor. Soc.*, **77**, 1275–1277.

Lin, H., and G. Brunet, 2018: Extratropical response to the MJO: Nonlinearity and sensitivity to the initial state. *J. Atmos. Sci.*, **75**, 219–234, doi: 10.1175/JAS-D-17-0189.1.

Liu, D. Q., and X. Q. Yang, 2010: Mechanism responsible for the impact of Madden–Julian Oscillation on the wintertime rainfall over eastern China. *Scientia Meteor. Sinica*, **30**, 684–693, doi: 10.3969/j.issn.1009-0827.2010.05.016. (in Chinese)

Madden, R. A., and P. R. Julian, 1971: Detection of a 40–50 day oscillation in the zonal wind in the tropical Pacific. *J. Atmos. Sci.*, **28**, 702–708, doi: 10.1175/1520-0469(1971)028<0702:DOADOI>2.0.CO;2.

Madden, R. A., and P. R. Julian, 1972: Description of global-scale circulation cells in the tropics with a 40–50 day period. *J. Atmos. Sci.*, **29**, 1109–1123, doi: 10.1175/1520-0469(1972)029<1109:DOGSCC>2.0.CO;2.

Ren, H.-L., and Y. Y. Shen, 2016: A new look at impacts of MJO on weather and climate in China. *Adv. Meteor. Sci. Technol.*, **6**, 97–105. (in Chinese)

Ren, H.-L., and P. F. Ren, 2017: Impact of Madden–Julian oscillation upon winter extreme rainfall in southern China: Observations and predictability in CFSv2. *Atmosphere*, **8**, 192, doi: 10.3390/atmos8100192.

Ren, P. F., H.-L. Ren, J.-X. Fu, et al., 2018: Impact of boreal summer intraseasonal oscillation on rainfall extremes in southeastern China and its predictability in CFSv2. *J. Geophys. Res. Atmos.*, **123**, 4423–4442, doi: 10.1029/2017JD028043.

Shao, X. L., S. L. Li, N. Liu, et al., 2018: The Madden–Julian oscillation during the 2016 summer and its possible impact on rainfall in China. *Int. J. Climatol.*, **38**, 2575–2589, doi: 10.1002/joc.5440.

Wang, H., F. Liu, B. Wang, et al., 2018: Effects of intraseasonal oscillation on South China Sea summer monsoon onset. *Climate Dyn.*, **51**, 2543–2558, doi: 10.1007/s00382-017-4027-9.

Wang, J. B., Z. P. Wen, R. G. Wu, et al., 2017: The impact of tropical intraseasonal oscillation on the summer rainfall increase over southern China around 1992/1993. *Climate Dyn.*, **49**, 1847–1863, doi: 10.1007/s00382-016-3425-8.

Wu, J. J., Z. J. Yuan, Y. K. Qian, et al., 2009: The role of intraseasonal oscillation in the southern-China snowstorms during January 2008. *J. Trop. Meteor.*, **25**, 103–111, doi: 10.3969/j.issn.1004-4965.2009.Z1.012. (in Chinese)

Xavier, P., R. Rahmat, W. K. Cheong, et al., 2014: Influence of Madden–Julian Oscillation on Southeast Asia rainfall extremes: Observations and predictability. *Geophys. Res. Lett.*, **41**, 4406–4412, doi: 10.1002/2014GL060241.

Yuan, W., and H. J. Yang, 2010: On the modulation of MJO to the precipitation of Southeast China in winter season. *Acta Sci. Nat. Univ. Pekinensis*, **46**, 207–214, doi: 10.13209/j.0479-8023.2010.030. (in Chinese)

Zhang, C. D., 2013: Madden–Julian oscillation: Bridging weather and climate. *Bull. Amer. Meteor. Soc.*, **94**, 1849–1870, doi: 10.1175/BAMS-D-12-00026.1.

Zhang, L. N., B. Z. Wang, and Q. C. Zeng, 2009: Impact of the Madden–Julian oscillation on summer rainfall in Southeast China. *J. Climate*, **22**, 201–216, doi: 10.1175/2008JCLI1959.1.

Zhang, L. N., P. F. Lin, Z. Xiong, et al., 2011: Impact of the Madden–Julian Oscillation on pre-flood season precipitation in South China. *Chinese J. Atmos. Sci.*, **35**, 560–570, doi: 10.3878/j.issn.1006-9895.2011.03.15. (in Chinese)

Zheng, C., and E. K.-M. Chang, 2020: The role of extratropical background flow in modulating the MJO extratropical response. *J. Climate*, **33**, 4513–4536, doi: 10.1175/JCLI-D-19-0708.1.

Tech & Copy Editor: Qi WANG